Collisional quenching and depolarization of NO_2 $\tilde{A}\,^2B_2$ state fluorescence as studied by Zeeman quantum beat spectroscopy

P. J. Brucat and R. N. Zare
Department of Chemistry, Stanford University, Stanford, California 94305

(Received 18 January 1984; accepted 24 May 1984)

We have studied the effect of collisions on the time-resolved fluorescence arising from a single optically selected fine structure level ($F_1 3_{03}$) of the $\tilde{A}\,^2B_2$ state of NO_2 prepared via absorption near 5933 Å in the presence of a weak magnetic field. The fluorescence modulation induced by the magnetic field (Zeeman quantum beats) is used to monitor the time dependence of the alignment. The alignment decays exponentially and follows simple Stern–Volmer kinetics. The incoherent fluorescence intensity, used to determine population information, fits well a bi-exponential form at nonzero pressure. This is interpreted by a simple kinetic scheme involving cascade to additional fluorescing states. We find that only about 15% of the population removed from the initial level by collision produces subsequent emission that is detected (630–830 nm). We are unable to identify the exact nature of these emitting states. However, it is clear that pure rotationally inelastic collisions do not dominate the energy transfer process. Collisional population and alignment relaxation rate constants for the optically prepared level have been measured for excited state collisions with He, Ne, Ar, Kr, Xe, N_2, CO, and NO_2 at 295 K and low density ($< 1 \times 10^{15}$ particle/cm^3). In particular, we find that the rate for population removal of the initially excited level by collision is faster than the rate for elastic disalignment (depolarization within the same rotational level).

I. INTRODUCTION

The low-lying (< 4 eV) excited states of NO_2 have demonstrated exceedingly complex and irregular behavior in almost all properties measured. Even in the isolated molecule, the interleaving of dense manifolds of rovibronic levels of grossly different nature makes high-resolution optical spectroscopy a difficult challenge. The description of these electronic states is of fundamental importance to the detailed understanding of photochemical and photocatalytic processes in the stratosphere, as well as the intermediate goal of modeling laboratory reactions involving the production or destruction of excited NO_2.

Because of the complexity and importance of excited NO_2, it is not surprising that the study of fluorescence quenching in this system has a long and controversial history. Early investigators attempted to characterize fluorescence kinetics in spite of the lack of quantitative spectroscopic data or quantum-state-specific preparation and detection techniques.[1] As experimentation advanced, the complexity and subtlety of the behavior of the collisionally perturbed NO_2 became more evident. Several generally accepted features of the system were gradually brought forth. First, the radiative lifetime of optically excited NO_2 was found to be long[2–4] and to vary irregularly from level to level.[5–10] This has been rationalized as evidence for extensive intramolecular coupling of the electronic states nearby in energy to the excited level in the isolated molecule.[11] Second, collisional quenching studies show large rates for vibrationally inelastic processes relative to that for simple electronic quenching,[12–19] complicating the fluorescence at finite pressure because of emission from levels populated by cascade. The final state of these inelastic events remains unknown.

Of particular interest to us are the specific collisional relaxation and energy transfer processes available to the optically prepared molecule. In this study we probe the fate of a single rotational level in time via its characteristic fluorescence as it suffers collisions with foreign gasses. The Zeeman quantum beat (ZQB) method[20] is used to monitor the state-specific alignment of the initial level. This method utilizes the spatially anisotropic fluorescence pattern from an ensemble of molecules excited with a pulse of polarized light in conjunction with the precessional motion of the ensemble in a magnetic field to produce a temporal modulation of the observed fluorescence intensity. The amplitude of this modulation represents the excited molecular alignment in the precessional frame. The frequency of the modulation is dependent on the energy splitting of the magnetic sublevels of the excited state induced by the field and is, in general, different for each upper state. The state-specific alignment information obtained by this method provides insight into the collisional fate of one initially prepared level and does not represent the average relaxation properties of excited NO_2 in general.

II. EXPERIMENTAL

The experimental apparatus and techniques used in this study have been described previously.[20] Briefly, an extracavity amplitude-modulated single-mode dye laser (peak power 30 mW; 150 ns duration rectangular pulse of a repetition rate of 5 KHz; free running bandwidth 50 MHz) is used to excite a gas-phase NO_2 sample at 295 K. The gas sample is a conduction-limited slow flow maintained in a region of an applied homogeneous magnetic field (0–20 G). The excitation pulse selectively prepares a single rovibronic level in the

 0021-9606/84/182562-09$02.10

$\tilde{A}\,^2B_2$ state whose fluorescence is detected at right angles through a polarizer/cutoff filter combination by an S20 response photomultiplier tube (Centronix QA4283 SA-25). The fluorescence signal is time resolved as a 1024 point array (resolution element 156 ns) by a discriminator TPHC/MCA combination and stored by a microcomputer on a floppy disk. The raw data are routinely corrected for pulse pileup, base line offset, and finite excitation pulse duration. The data are analyzed in the form of a $\ln[I(t)/I(t=0)]$ vs time plot and a 1024 point complex Fourier transform of the time decay.

The NO_2 sample is obtained from trap-to-trap distilled (snow white crystalline powder at 77 K) Matheson 99.5% pure NO_2 stored in a glass and Teflon bulb. The buffer gasses (He, Matheson, 99.995%; Ne, Matheson, 99.99%; Ar, Matheson, 99.998%; Kr, Spectra Gasses, 99.995%; Xe, Spectra Gasses, 99.999%; N_2, Liquid Carbonic, 99.996%; CO, Matheson, 99.5%) were used without further purification. Pressure measurements for these studies were carried out by use of a capacitance manometer (Baratron 220B 1 Torr absolute head, PDR-C-1B controller) calibrated by the manufacturer. Observed fluorescence and excitation spectra taken at the same total pressure and various flow rates from near static to 20 1/s indicated that thorough mixing and thermal equilibrium were maintained under these conditions. Total pressures were stable to within $\pm 1\times10^{-4}$ Torr over periods of hours.

The overall detector wavelength response spans only a fraction of the emission expected from the optically excited sample. Figure 1 shows an approximate detection efficiency vs wavelength curve derived from the transmission curves of the various elements in the detector's optical train and the manufacturer's specifications for the PMT.

Because of the long emission lifetime encountered in this study, the excitation/detection geometry and emitter effusion/diffusion must be specifically considered to avoid systematic errors. A temporal bias in the detection efficiency occurs when the emitting species produced in the laser volume live long enough for their thermal motion to remove them from the detection volume, causing the probability of the detection of emission at later times to be reduced relative to that at earlier times. This effect has been discussed specifically with regard to the investigation of NO_2 fluorescence.[5,7] Ideally, one would choose to perform the experiment with a small excitation spot centered in a large region of homogeneous detection sensitivity to provide a minimum in temporal detection bias. This limit was approached in the work of Donnelly and Kaufman[8,9,18,19] who employed a 72 ℓ spherical bulb in which excited molecules could travel 18 cm before leaving the field of view of the detector. Practical considerations often make this situation difficult to achieve for very long lifetimes or fast thermal motion.

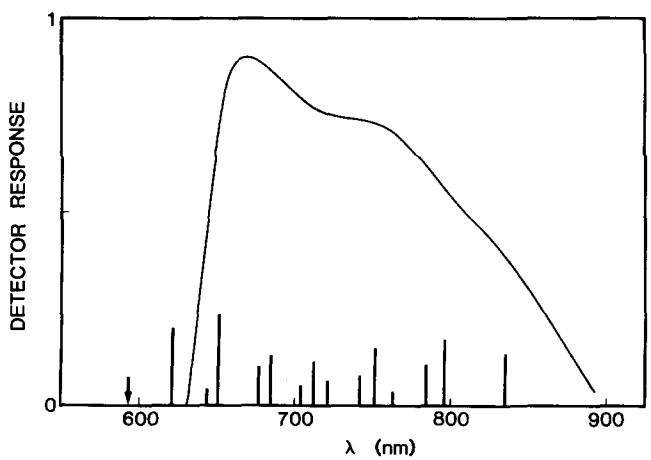

FIG. 1. Overall detector response vs emission wavelength. The arrow indicates the laser excitation and the bars represent some of the prominent NO_2 fluorescence features associated with the level studied. The entire fluorescence spectrum continues an undetermined extent further to the red.

In this study, the dimensions of the emission volume are restricted by field inhomogeneity constraints and we were forced therefore to develop an alternative method of correction for the systematic errors in detection caused by the use of a limited field of view. At very low gas density (no collisions), the effect of the free effusion of the emitting species may be calculated easily for a given excitation/detection geometry. The light collection efficiency of the detection system is first measured or estimated as a function of distance from the excitation zone. This is then recognized as a collection efficiency vs velocity relationship at a given delay time from excitation. Thus, the fractional detection probability of the ensemble of emitters at any time is obtained by an average over the thermal velocities in the gas.

The excitation region in this experiment is a stripe (about 2 mm high and 10 mm wide) of collimated laser light whose length is large compared to all other pertinent dimensions. The detection is performed at right angles to the laser light propagation and is restricted in field of view compared to the distance between the detector and the excitation zone. Thus, emitter motion along the excitation stripe or along the detection direction is not so important to the fluorescence collection efficiency as the motion perpendicular to these directions. Moreover, the detection response to a light source translated in this latter direction falls off rather smoothly from a plateau of near unity response close to the excitation zone. The solid curve in Fig. 2 shows the natural logarithm of the normalized temporal detection bias $\ln[f_D(t)]$, calculated for NO_2 at 295 K, excited in the center of a one-dimensional Gaussian detection region whose $1/e$ falloff points are separated by 5.6 cm. The points in Fig. 2 are an experimental estimation of the $\ln[f_D(t)]$ obtained from the observed decay waveform of several NO_2 $\tilde{A}\,^2B_2$ levels of different known lifetimes at very low pressure. The agreement between this model calculation and experiment for short times ($t < 30\,\mu$s) can be improved by the inclusion of a plateau region in the spatial detection response function near the excitation zone but this procedure has the drawback of introducing another adjustable parameter in the model and hence was not carried out.

The ability to fit experimental and model $f_D(t)$ functions for several detection geometries and emitter lifetimes gives us confidence that we can successfully parametrize the effect of emitter effusion in the limit of collisionless conditions. As the gas density is increased in the sample cell, velocity-changing collisions will inhibit the escape of the emitting molecules from the detection volume increasing the detection efficiency at long times relative to the low density case. Thus the free effusion case gives a **lower limit** to $f_D(t)$ at

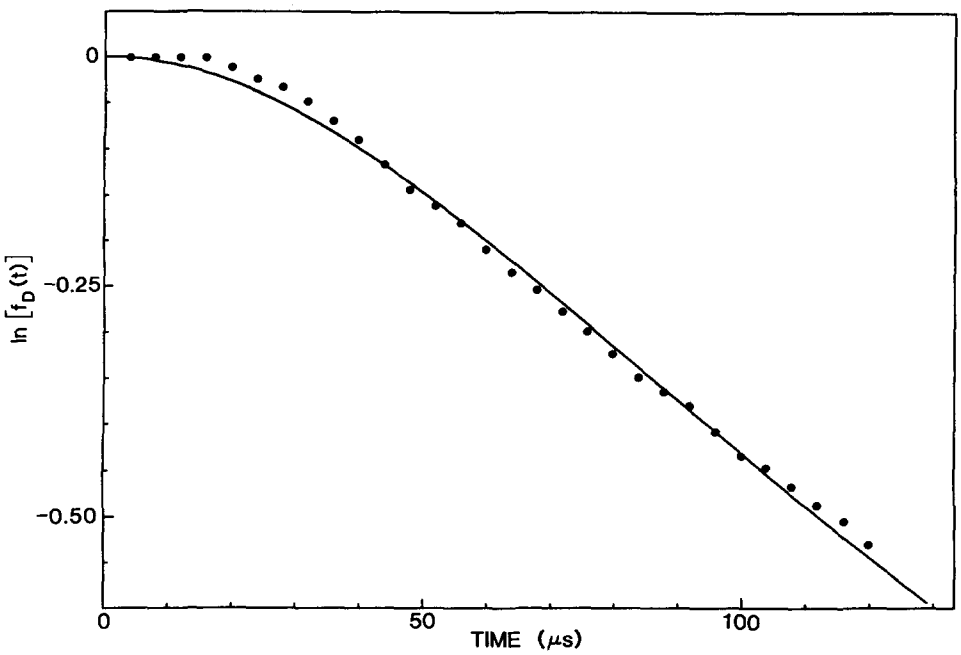

FIG. 2. The logarithm of the normalized detection bias $\ln[f_D(t)]$ vs time. The points are experimental and solid curve is a model calculation.

any time. The transition between regimes where effusion is important and that where velocity-changing collisions dominate is earmarked by positive curvature at low density in a plot of the effective radiative rate vs pressure. This is caused by the functional dependence of $f_D(t)$ on pressure, which we have not attempted to characterize. If the consequence of emitter effusion/diffusion were ignored [$f_D(t)$ assumed to be unity], the error in the effective radiative rate at low pressure would be on the order of the slope of the best line through the curve of Fig. 2, i.e., about $5\times10^3\ s^{-1}$. Furthermore an error is introduced in the determination of the slope of the effective radiative rate vs pressure, causing slower bimolecular rate constants to be more poorly determined than faster ones.

III. RESULTS

We present the results of collisional time-resolved fluorescence studies of the selectively excited $F_1 3_{03}$ rotational level of the $\tilde{A}\ ^2B_2$ electronic state of NO_2 at a term energy of 16 854.50 cm^{-1}. This level is accessed through either the $P_1(4)$ or $R_1(2)$ members of the prominent, although vibrationally unassigned, vibronic band at 5933 Å, dubbed No. 99 by Smalley *et al.*[21] We have also performed similar, although less extensive, experiments on nearby rotational levels of the same vibronic band and the results of those studies are qualitatively identical to those presented here.

As described before,[20] the magnetic field-induced modulation of fluorescence polarization provides a direct measure of the alignment (or orientation) of the emitting level. This Zeeman quantum beat signal arises from the coherence between the magnetic sublevels of the aligned excited state whose energy splitting is "tuned" by the applied magnetic field. As the coherence between these sublevels is destroyed the signal is damped. The evolution of the excited state alignment (sublevel coherence) is represented in the decay envelope of the beat pattern in time, or equivalently (through the Fourier transform) in the line shape of the beat in frequency.

In the absence of collisions or other extrinsic relaxation processes, the line shape of the beat signal is Lorentzian with a linewidth determined by the spontaneous decay rate of the emitting level. In this situation, the half-width at half-maximum of this Lorentzian Γ_2 is equal to $\Gamma_0 = (2\pi\tau_0)^{-1}$, where τ_0 is the radiative lifetime. Collisions relax the alignment as well as remove population from the emitting level and $\Gamma_2 = \Gamma_2^* + \Gamma_0$, where Γ_2^* is proportional to the pure elastic disalignment rate. The conditions of our experiment are such that the duration of the average collision is much shorter than the precessional period of the emitting state in the magnetic field. This causes the relative collision velocity to be isotropic when transformed into the precessional frame.[22] Hence the measurement of the rate of disalignment in this frame by the method of field-induced quantum beats is equivalent to a measurement in the laboratory-fixed frame.

Figure 3 is the normalized real part of the Fourier transform of the time decay called the ZQB spectrum. It shows the beat frequencies of the three hyperfine components ($F' = 9/2, 7/2, 5/2$) of the $F_1 3_{03}(J' = 7/2)$ level in a 1.7 G magnetic field at two different total sample pressures. In each case, the experimental beat line shape well fits a Lorentzian (i.e., the effective alignment decays exponentially in time) and a value of Γ_2 is determined from the fit. The value of Γ_2 at a given pressure is always found to be the same for each of the hyperfine (F') levels belonging to a single fine structure (J') level. This linewidth is not dependent on the magnitude of the applied magnetic field to within experimental error. In addition, no "satellite" or collisionally induced quantum beats are observed at any pressure. From the foreign gas density dependence of Γ_2, a collisional disalignment rate constant k_A is determined. For a given buffer gas, Γ_2 obeys the relationship

$$\Gamma_2([M]) = k_0 + \Delta + k_A[M], \tag{1}$$

where $[M]$ is the density of the foreign gas, $k_0 = 1/\tau_0$ is the collisionless spontaneous relaxation rate of the excited level,

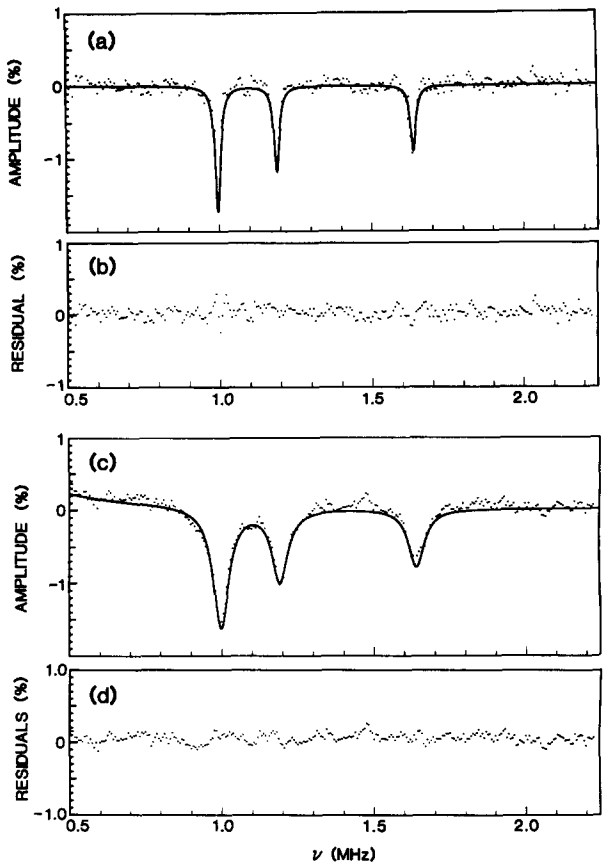

FIG. 3. The real part of the Fourier transform of the pulsed excited emission (ZQB spectrum) of the $F_1 3_{03}$ level at different total sample pressures: (a) pure NO_2 at 1.3×10^{-3} Torr; and (c) pure NO_2 at 7.5×10^{-3} Torr. Both spectra were taken at 1.7 G under otherwise identical conditions. The corresponding residuals shown in (b) and (d) are the difference between the experimental points and the Lorentzian fit (solid curve).

and Δ is a pressure-independent magnetic field inhomogeneity term. The rate constant k_A encompasses all collisional processes that remove alignment *or* population from the ensemble of excited molecules.

We now consider the collisional rate constant for the removal of population alone from the laser excited level k_P. Figure 4 shows the decay envelope for total emission following pulsed excitation of the $F_1 3_{03}$ level at finite pressure. The decay is markedly nonexponential and the corresponding line shape (shown in the inset) is non-Lorentzian. Transverse relaxation of the alignment of the excited ensemble that does not precess in the magnetic field ($\langle T^{\dagger}_{20}\rangle$[23]) complicates the direct extraction of the evolution of population from the decay envelope. Correction for this effect in this case is, however, numerically insignificant due to the small degree to which $\langle T^{\dagger}_{20}\rangle$ contributes to the overall decay[20] and the similar time dependences of the population and effective alignment of the initial level. The observed decay envelopes are found to fit well a biexponential form

$$I_E(t) = I_E(0)[(1-C)\exp(-R_0 t) + C\exp(-R_1 t)] \tag{2}$$

over the entire pressure range studied (typically 0.5–15 mTorr).

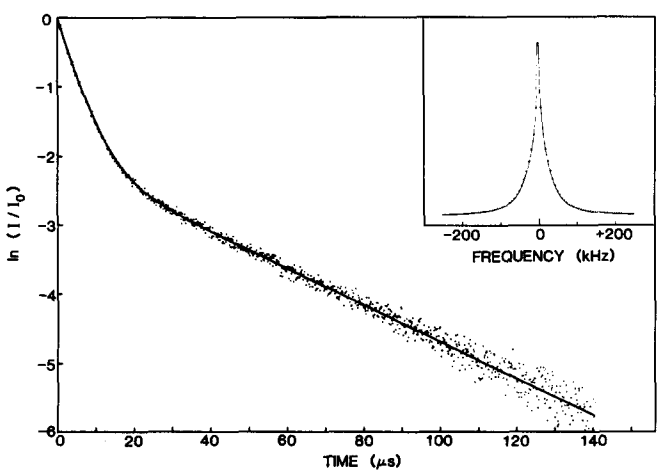

FIG. 4. The logarithm of the normalized overall emission intensity vs time and the corresponding Fourier transform (inset). The experimental decay envelope (points) is fit to a biexponential form (solid curve) using Eq. (2). The spectrum was taken at an NO_2 pressure of 5×10^{-5} Torr and N_2 pressure of 1.12×10^{-2} Torr.

This biexponential form of the decay implies the presence of two classes of states $\mathbf{N}_0$, and $\mathbf{N}_1$, both contributing to the total emission. While one is able to characterize $\mathbf{N}_1$ by properties averaged over all levels that act as $\mathbf{N}_1$, this does not allow us to understand the properties of individual $\mathbf{N}_1$ levels. The foreign gas density dependence of the parameters R_0, R_1, and C is consistent with a simple kinetic scheme involving collisional cascade between the populations N_0 and N_1. This scheme is diagrammed as follows:

$$\begin{array}{ccccc} X & \xleftarrow{k_4[M]} & N_0 & \xrightarrow{k_0} & X + h\nu_0 \\ & & \downarrow{\scriptstyle k_3[M]} & & \\ X & \xleftarrow{k_5[M]} & N_1 & \xrightarrow{k_1} & X + h\nu_1 \end{array} \tag{3}$$

where k_0 and k_1 are the spontaneous emission rates from $\mathbf{N}_0$ and $\mathbf{N}_1$, and $\mathbf{X}$ denotes all undetected final states. The states $\mathbf{X}$ are unknown and need not be exclusively associated with levels of the ground state. Here, the population removal rate from $\mathbf{N}_0$, k_P is identified as $k_3 + k_4$. As will become clear from what follows, the model shown in Eq. (3) well describes the behavior of $\mathbf{N}_0$, but fails in detail for $\mathbf{N}_1$, apparently because of the inadequacy of representing the class of states $\mathbf{N}_1$ with the parameters corresponding to a single state.

The solution to the set of coupled differential equations implied by Eq. (3) subject to the initial conditions of $N_0 = 1$ and $N_1 = 0$ is

$$\begin{aligned} N_0(t) &= \exp\{-[k_0 + (k_3 + k_4)[M]]t\}, \\ N_1(t) &= Q([M])(\exp[-(k_1 + k_5[M])t] \\ &\quad - \exp\{-[k_0 + (k_3 + k_4)[M]]t\}), \end{aligned} \tag{4}$$

where

$$Q([M]) = k_3[M]/[(k_0 - k_1) + (k_3 + k_4 - k_5)[M]]. \tag{5}$$

The observed fluorescence decay signal is the rate of detection of $(h\nu_0 + h\nu_1)$ at time t after excitation. However, all emitting states are not observed with equal detectivity. In particularly, fluorescence from collisionally populated levels $\mathbf{N}_1$ are expected to be more red shifted than fluorescence from $\mathbf{N}_0$.[1,5,12,16,18] Hence we introduce the relative detecti-

vity factor d_1, which expresses the ratio of the detector response to fluorescence from N_1 compared to N_0. In terms of the cascade model shown in Eq. (3), the ensemble photon emission rate is then given by

$$\begin{aligned} I(t;[M]) &= k_0 N_0(t) + d_1 k_1 N_1(t) \\ &= [k_0 - d_1 k_1 Q([M])] \\ &\quad \times \exp\{-[k_0 + (k_3 + k_4)[M]]t\} \\ &\quad + d_1 k_1 Q([M]) \exp[-(k_1 + k_5[M])t]. \end{aligned} \tag{6}$$

The parameters R_0, R_1, and C in the phenomenological form of the decay [Eq. (2)] can now be identified in terms of the constants in Eq. (6):

$$\begin{aligned} R_0 &= k_0 + (k_3 + k_4)[M], \\ R_1 &= k_1 + k_5[M], \\ C &= \frac{d_1 k_1 Q([M])}{k_0} = \frac{d_1 k_1 k_3 [M]}{k_0} (R_0 - R_1)^{-1}. \end{aligned} \tag{7}$$

The values of R_0, R_1, and C are found to follow the foreign gas density dependence of Eq. (7) to within experimental error for all gasses and for all pressure ranges studied. Here, R_0 has been corrected for emitter effusion/diffusion at low pressure as discussed in Sec. II. For a given foreign gas, the rate constants k_0, $(k_3 + k_4)$, k_1, and k_5 are derived from the intercept and slope of the linear least squares fit to the R_0 vs $[M]$ and R_1 vs $[M]$ data (see Fig. 5). Then the C vs $[M]$ data yield the value of $d_1 k_3$, but without a knowledge of d_1 it is not possible to determine separately k_3 and k_4. However, the reasonable assumption that d_1 is less than unity, i.e., that N_0 is detected preferentially to emission from N_1, allows us to place lower and upper bounds on k_3 and k_4, respectively.

It remains to identify the populations N_0 and N_1 and combine the information obtained from the ZQB line shape with that obtained from the incoherent fluorescence decay envelope. Because no collisional transfer of alignment and precessional phase to other emitting levels is observed, the population N_0 is subdivided into those molecules that are aligned, ${}^A N_0$, and those unaligned, ${}^U N_0$, where $N_0 = {}^A N_0 + {}^U N_0$. The kinetic model diagrammed in Eq. (3) is then modified to include ${}^A N_0$ and ${}^U N_0$:

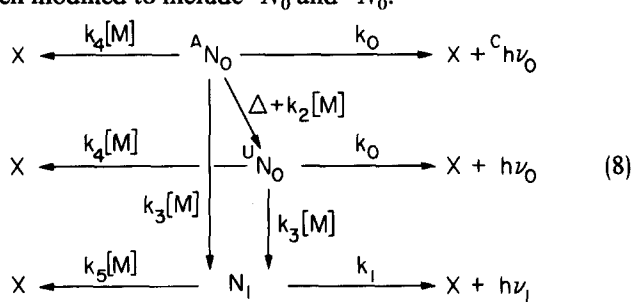

(8)

where ${}^C h\nu_0$ denotes coherent emission. The time dependence of the populations N_0 and N_1 in Eq. (8) are the same as in Eq. (3), i.e., they are given by Eq. (4) subject to the analogous initial conditions. In addition, the time dependence of the laser excited alignment follows the form:

$${}^A N_0(t) = {}^A N_0(0) \exp[-(k_0 + \Delta + (k_2 + k_3 + k_4)[M])t]. \tag{9}$$

The collisional rate constant determined from ZQB line broadening, k_A, is then identified as

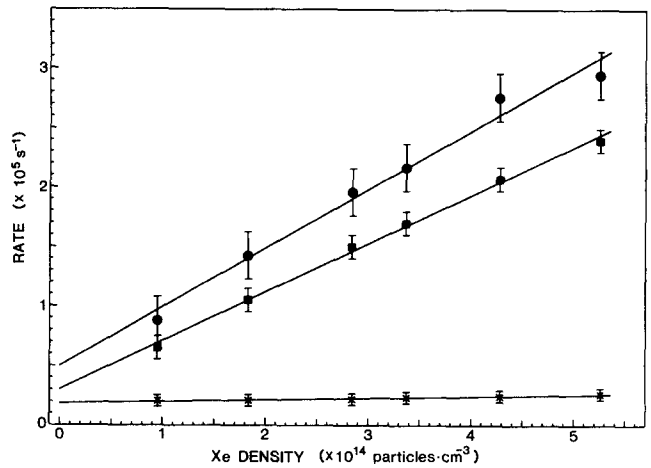

FIG. 5. Experimental rate (points) vs foreign gas (xenon) density with linear least squares fit to the data(line). Circles: Γ_2; squares: R_0; crosses: R_1. The error bars correspond to what is believed to be a 95% confidence limit. The zero pressure intercepts of the R_0 vs $[M]$ and Γ_2 vs $[M]$ lines differ by the rate Δ, which is proportional to the (pressure-independent) magnetic field inhomogeneity.

$$k_A = k_2 + (k_3 + k_4). \tag{10}$$

The ZQB measurement of the rate k_A is used to find k_2, the rate for pure collisional disalignment, knowing $k_P = k_3 + k_4$. This completes the determination of the constants in Eq. (8).

Table I shows the rate constants measured for various collision partners with the $F_1 3_{03}$ level of NO_2. The directly observed rate constants k_A and $k_P = (k_3 + k_4)$ show an expected but "mild" dependence on the identity of the collision partner with a trend of increasing rates for more complex partners. The near equality of k_P and k_A for a given gas in Table I shows immediately that pure elastic disalignment does not dominate the thermal collision process. Note that an exact equality between the decay time of the ZQB signal and $1/R_0$ would lead to the strict identification of the class of levels N_0 with the laser excited (initial) level. A **lower limit** to the fraction of the emission from N_0 arising from the initial level is $R_0/(R_0 + k_2[M])$. At high pressure, this lower limit varies from 65% for CO to 93% for Ne, strongly implying that the initial level is entirely responsible for the short lifetime component of the observed fluorescence.

Figure 6 shows the different relative probabilities of collision-induced events available to the initial level for various foreign gasses. Here the rates k_A are subdivided into pure disalignment k_2 and population removal k_P by direct quenching k_4 and cascade to emissive states k_3. The fraction of the population removed from the initial level cascaded to levels whose emission is detected $d_1 k_3/(k_3 + k_4)$ appears to be 15% and to be independent of quenching gas. The fraction of elastic to total effective disalignment $k_2/(k_2 + k_3 + k_4)$ is largest for CO and N_2 and anomalously small for NO_2 and Ne.

The rate constants k_1 and k_5 determined for N_1 are more uncertain than corresponding rates for N_0 because of temporal detection bias discussed in Sec. II. Hence these rates should be regarded more as fitting parameters rather than significant quantities intrinsic to the molecule. The examination of the relative quantum yield for fluorescence of the ensemble at finite pressure elucidates some of the short-

TABLE I. Rate constants for the $F_1 3_{03}$ level[a] of $\tilde{A}\,^2B_2\,NO_2$ at 16 851.98 cm^{-1} determined for the kinetic model diagrammed in Eq. (8). Bounds of k_3 and k_4 are based on the assumption that $d_1 \leq 1$.

Gas	(k_3+k_4)[b]	k_A[b]	k_1[c]	k_2[b]	k_3[b]	k_4[b]	k_5[b]
He	3.0 ± 0.2	3.9 ± 0.5	2.0	0.9	>0.48	<2.5	0.08
Ne	2.6 ± 0.7	2.8 ± 1.0	2.1	0.2	>0.40	<2.2	0.08
Ar	3.8 ± 0.7	5.0 ± 1.0	2.1	1.2	>0.58	<3.3	0.03
Kr	3.7 ± 0.7	4.2 ± 1.0	2.1	0.5	>0.61	<3.1	0.02
Xe	4.1 ± 0.3	4.9 ± 0.5	1.9	0.8	>0.60	<3.5	0.02
N_2	4.6 ± 0.3	6.3 ± 1.0	2.0	1.7	>0.69	<3.9	0.17
CO	4.9 ± 0.3	7.5 ± 1.0	2.0	2.6	>0.77	<4.2	0.19
NO_2	5.9 ± 0.5	6.5 ± 0.5	1.8	0.6	>0.87	<5.0	0.53

[a] $k_0 = 1.9(2) \times 10^4\ s^{-1}$.
[b] In units of $10^{-10}\ cm^3$/particle s.
[c] In units of $10^4\ s^{-1}$.

comings of the simple two-population model described so far. Figure 7(a) presents the total emission intensity of the sample at finite buffer gas (helium) density relative to that at zero buffer gas density $\Phi_{TOTAL}([M])$. In the context of the model depicted in Eq. (8), $\Phi_{TOTAL}([M])$ may be calculated from the constants in Table I according to

$$\Phi_{TOTAL}([M]) = \Phi_0([M]) + \Phi_1([M]), \tag{11}$$

where

$$\Phi_0([M]) = \frac{k_0}{k_0 + (k_3 + k_4)[M]} \tag{12a}$$

and

$$\Phi_1([M]) = d_1 k_1 Q([M]) \left[\frac{1}{k_1 + k_5[M]} - \frac{1}{k_0 + (k_3 + k_4)[M]} \right] \tag{12b}$$

are the contributions to Φ_{TOTAL} arising from N_0 and N_1, respectively. We do not know the relative detection response factor d_1 but believe that $d_1 \leq 1$. Let us begin by taking $d_1 = 1$. With this assumption Fig. 7(a) shows that Eq. (11) *does not adequately describe the pressure dependence of* Φ_{TOTAL}, but that the observed relative quantum yield approaches the partial quantum yield from N_0 at high densities. Moreover, no simple scaling in which d_1 is set equal to some fraction less than unity can rectify this gross failure of the model. Figure 7(b) presents the experimental Φ_{TOTAL} minus the calculated Φ_0. This is compared to the value of Φ_1 calculated from Eq. (12b) for $d_1 = 1$. Again this comparison is suggestive that d_1 needs to be made pressure dependent presumably caused by increased red-shifted fluorescence with increasing number of collisions, i.e., the behavior of N_1 cannot be described by a single set of density-independent properties. Of course, an immediate corollary to this conclusion is that the rate constants pertaining to the class of levels N_1 that we have derived are not very meaningful, in contrast to those for N_0.

IV. DISCUSSION

The interpretation of pseudo-first-order rate constants for the effect of collisional processes on resonance fluorescence has many complications. In addition to the well-known problems associated with averages over thermal ensembles and multiple collisions, there is the further complexity of NO_2, itself, whose excited state structure resists simple description and whose levels show large variabil-

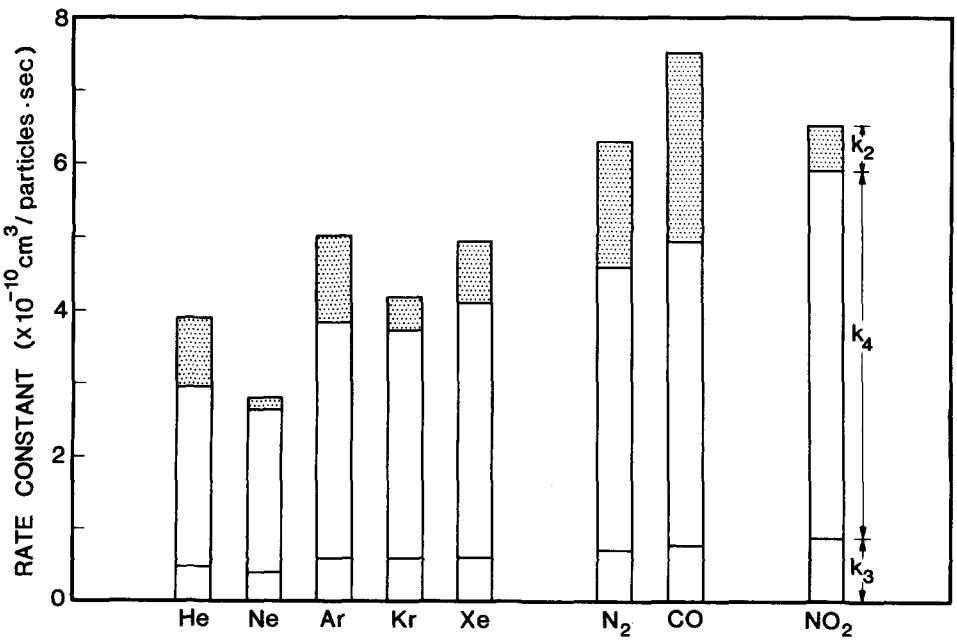

FIG. 6. A histogram of bimolecular rate constants $k_A = k_2 + (k_3 + k_4)$ vs foreign gas, where k_2 is the pure disalignment rate constant, k_3 is the cascading rate constant, and k_4 is the direct quenching rate constant. The values of k_3 and k_4 are lower and upper bounds, respectively (see Table I), while their sum, $k_P = (k_3 + k_4)$ is determined unambiguously.

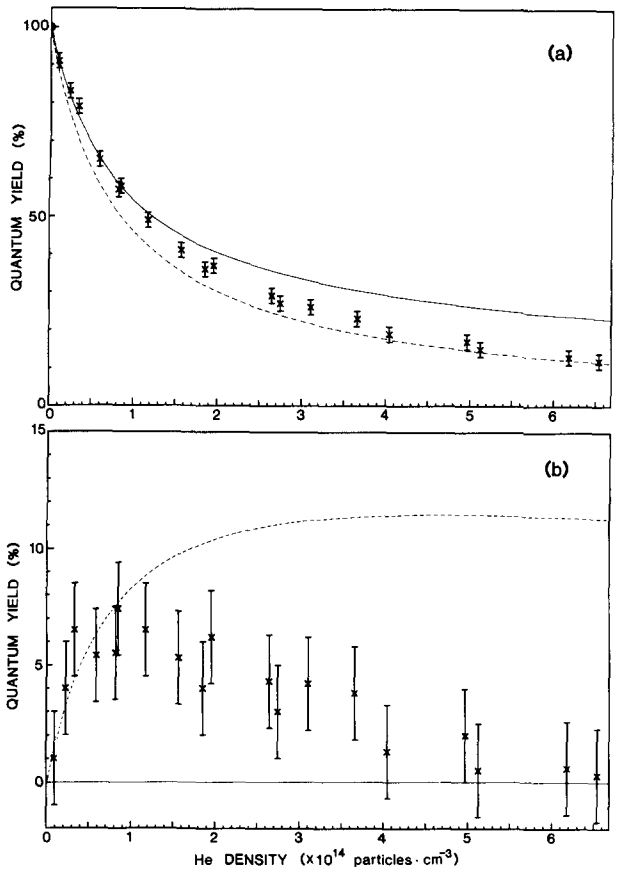

FIG. 7. Quantum yield for total emission relative to zero pressure as a function of helium density. (a) total quantum yield. Crosses: experimental data; Solid curve: total quantum yield calculated from Eq. (11) for $d_1 = 1$; Dashed curve: partial quantum yield from N_0 calculated from Eq. (12a). (b) Partial quantum yield for cascaded emission. Crosses: experimental total quantum yield minus calculated partial quantum yield from N_0; Dashed curve: partial quantum yield of N_1 calculated from Eq. (12b) for $d_1 = 1$. All calculated curves are obtained from the unadjusted He rate constants of Table I.

ity in radiative lifetime, emission wavelengths, and other properties. There have been extensive studies of the excited state kinetics of NO_2, and we call the reader's attention to the thorough investigation of Donnelly and Kaufman.[8,9,18,19] They determined fluorescence lifetimes and quenching rates for a number of features in the NO_2 visible spectrum. Using a pulsed dye laser or the fixed frequency-doubled lines of a Nd:YAG laser, they observed the NO_2 fluorescence in different bulb geometries with time and wavelength resolution as a function of pressure of various gases. Their observations represent an average over different excited state levels weighted by their absorption line strength. These studies are useful in characterizing the behavior of optically excited NO_2 over a narrow bandwidth but in no sense represent the behavior of a single well characterized level. In contrast, this study concerns one level, the F_1 spin component of the 3_{03} level at a term energy of 16 854.50 cm^{-1} above the lowest level of the ground state. This level is far from typical, being the upper level of one of the strongest lines in the so-called 593.3 nm band (No. 99). Consequently, it is difficult to make a direct comparison between the results of the present study on a single level and those of previous work on distributions of levels. Moreover, the present study provides new information on the collisional behavior of excited NO_2, namely, the collisional destruction of alignment. Nevertheless, where comparisons are possible, it appears that the present work is in accord with previous measurements, as will be discussed below.

For example, let us compare the radiative lifetime ($1/k_0$) and the quenching rate ($k_3 + k_4$) of the excited state level that we prepare with that prepared in the experiments of Donnelly and Kaufman. In the same excitation wavelength region, Donnelly and Kaufman[8] observe biexponential decays at their lowest pressures, the short component of which (45^{+11}_{-7} μs at 593.45 $\pm$ 0.05 nm) can be compared to our measured low-pressure single-exponential lifetime of 52^{+18}_{-0} μs. Similarly, at the same wavelength the collisional rate constant for removal of population from the state responsible for the short-lived emission for NO_2 self-quenching in Donnelly and Kaufman's work[8] is $5.9 \pm 0.5 \times 10^{-10}$ cm^3/particle s, which can be compared with our value of $(k_3 + k_4) = 5.9 \pm 0.5 \times 10^{-10}$ cm^3/particle s. Donnelly and Kaufman[18] have studied quenching with other gases using excitation at 532 nm with a 1 cm^{-1} bandwidth. They find the quenching rate constant of the "banded" fluorescence features, which they associate with the short-lived emission component, in units of 10^{-10} cm^3/particle s to be 3.29 ± 0.17 for He, 3.98 ± 0.14 for Ar, 4.58 ± 0.31 for N_2, and 5.93 ± 0.18 for NO_2. Our values of $(k_3 + k_4)$ for corresponding gases are 3.0 ± 0.2 for He, 3.8 ± 0.7 for Ar, 4.6 ± 0.3 for N_2, and 5.9 ± 0.5 for NO_2. Thus the agreement between the observed properties of N_0 and the observed properties of the banded fluorescence features of Donnelly and Kaufman[18] appear better than we expected.

However, the radiative and quenching properties of the set of levels we call N_1, and the states associated with the "continuum" emission in Donnelly and Kaufman's work are in rather poor agreement. First, let us consider the radiative properties of N_1. We find that the average radiative lifetime ($1/k_1$) is approximately that of the optically prepared level ($1/k_0$). Donnelly and Kaufman's[8] analysis shows that this behavior does not occur for the collectin of levels they excite near 593 nm ($\tau_C = 260 \pm 35$ μs for the continuum emission; $\tau_B = 70 \pm 10$ μs for the banded emission) but $\tau_B \simeq \tau_C$ for the collection of levels they excite near 532 nm.[19] We find that excitation *between* assigned strong features in the 593.3 nm band produces emission with an apparent decay rate so long as not to be reliably quantified ($\tau > 200$ μs) in our experiment. Consequently, we are unsure as to the validity of the comparison of zero pressure intercepts between the two studies for this band. Moreover, we can offer no certain explanation why collisions preferentially populate levels whose radiative behavior is similar to N_0. Clearly our experiment is biased toward the preferential observation of shorter lived rather than longer-lived emission, but we believe this cannot account fully for this difference. Possibly, the long-lived emission we see produced by excitation between sharp absorption features arises from high J' levels, whereas one or a few thermal collisions with the $F_1 3_{03}$ level may preferentially produce low J' levels, which could exhibit shorter-lived emission.

Finally, the apparent quenching rate constants of the levels we call N_1 do not mimic the findings of Donnelly and Kaufman for quenching of the continuum emission. As men-

tioned before, our rate constants k_5 should be regarded as phenomenological fitting parameters, which contain the uncharacterized pressure dependence of the temporal detection bias $f_D(t)$. Consequently, we make no further effort to refine this comparison.

Let us consider more deeply the kinetic scheme [Eq. (8)] which we have postulated to interpret our data. For this purpose, it is necessary to examine the role of multiple collisions. If each time an electronically excited A^* molecule collides with B complete removal of the excess electronic energy of A^* occurs, then the fluorescence rate and quantum yield depend only on the fraction of A^* that suffer **at least** one collision before emitting. This is a strong collision limit and can be treated by simple Stern–Volmer kinetics.[24] If, however, we study the effect of a "soft" collision, i.e., one in which the consequences of successive collisions are cumulative, the **number** of collisions the A^* suffers before emitting is relevant. Collisions causing partial disalignment or vibrational cascade without electronic quenching are examples of this kind of soft collision. The modeling of the consequences of multiple collision phenomena is the basis for all cascade kinetic schemes for this type of fluorescence quenching study. We may estimate the significance of the multiple collisions with regard to the overall fluorescence by the application of Poisson statistics.[25] This assumes that the collision events are uncorrelated, as is expected in our thermal ensemble. For a soft collision rate constant of k_S, a collisional population removal rate constant of k_P, and a spontaneous emission rate of k_E, the probability of A^* undergoing n and only n collisions before radiating is given by

$$P(n) = \beta^n/(1+\beta)^{n+1}, \tag{13}$$

where

$$\beta = \frac{k_S[M]}{k_E + k_P[M]}. \tag{14}$$

Here β is the ratio of the soft collision rate to the total rate of removal of A^*. Since this model assumes that an excited molecule can be removed by either emission or by direct quenching and that this can happen only once, β also represents the average number of soft collisions before emission, at a gas density of $[M]$. Figure 8 shows the form of $P(n)$ vs β for various collision numbers n. As β increases, the number of molecules undergoing two or more collisions, given by $\beta^2/(1+\beta)^2$, rapidly becomes appreciable. However, the dissection of the multiple collision processes into their constituent n-collision-event contributions cannot be carried out without some additional knowledge about the effect of sequential collisions, i.e., the study of collisional cascade as a function of density does not contain in itself a means of determining the microscopic effects of n-collision events but, instead, the average over such events.

Our measurement of the alignment of the initially excited fine structure level through the use of magnetic-field-induced quantum beats is not affected by alignment cascade or the transfer of alignment to other emitting levels. This is because the beat signal depends on the frequency of precession of the emitting state in the applied field and is thus state specific. In addition, any emitting levels that do retain alignment upon an inelastic collision do not give rise to a "satellite" quantum beat because the collision and laser pulse are uncorrelated in time, causing the ensemble average of the coherence transfered to the level to vanish. Since we monitor the alignment loss in an ensemble-averaged sense, we are unable to distinguish the successive partial removal of alignment from individual molecules from that of total disalignment upon each and every collision. Thus, the loss of alignment can be modeled in analogy to simple Stern–Volmer electronic quenching.

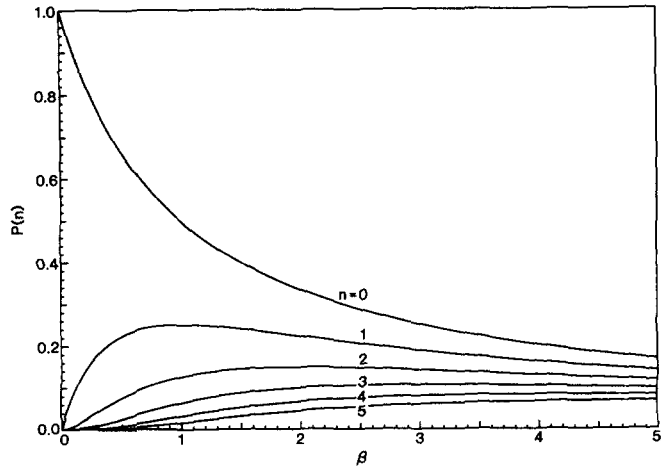

FIG. 8. A plot of the probability of an excited molecule undergoing n and only n soft collisions before radiating vs β, the average number of soft collisions before emission. See Eqs. (13), (14), and the accompanying text.

In contrast, the total population of emitting states derived from the incoherent fluorescence decay envelope shows marked signs of multiple collision effects. The success of our truncated (two-level) cascade scheme (8) in modeling low density fluorescence decays suggests that further consequences of multiple collisions will surface at higher densities. Without regard to the identity of the N_0 and N_1 levels, but merely using the lower limit ($d_1 = 1$) to the rate constant k_3 as an indicator of the cascade process, we may estimate the fraction of N_1 levels undergoing further cascade before emitting as

$$S = \frac{\sum_{n\geq 2} P(n)}{\sum_{n\geq 1} P(n)} = \beta/(1+\beta) = \frac{k_3[M]}{k_1 + (k_3 + k_5)[M]}. \tag{15}$$

Here we have used the results of Eqs. (13) and (14) and identified the soft collision rate constant k_S with k_3, the collisional population removal rate constant k_P with k_5, and the radiative decay rate k_E with k_1 (which approximately equals k_0). Table II shows the quantity S evaluated at various helium buffer gas pressures using the constants k_1, k_3, and k_5 from Table I. The fairly large estimated fraction of levels labeled as N_1 that undergo further (cascading) collisions before radiating indicates that the average nature and properties of N_1 change with pressure. This is exemplified by the failure of our truncated cascade scheme to describe both the fluorescence rate and quantum yield with a single set of rate constants for N_1. Figure 7(b) shows that the rate constants derived from the decay of N_1 emission vs density overestimate the quantum yield for emission of these levels. This is consistent with a picture of consecutive collisions modifying N_1.

TABLE II. Fraction S of N_1 levels undergoing collisions with He before emission at various pressures, calculated from Eq. (15).

Pressure (mTorr)	β^a	S
0	0.00	0.00
1	0.08	0.07
2	0.15	0.13
3	0.23	0.18
4	0.30	0.23
5	0.37	0.27
6	0.44	0.30
7	0.50	0.33
8	0.57	0.36
9	0.63	0.39
10	0.69	0.41
11	0.75	0.43
12	0.81	0.45
13	0.87	0.47
14	0.93	0.48
15	0.98	0.50
25	1.48	0.60
50	2.37	0.70
100	3.40	0.77
∞	6.00	0.86

[a] See Eq. (14).

The most probable interpretation is that the effect of subsequent collisions is to red shift the fluorescence wavelength of the N_1 emission, decreasing the overlap with the detector's wavelength response (Fig. 1) and thus reducing the detection efficiency of the N_1 levels as the pressure is increased. A collisionally induced red shift in fluorescence has been observed directly in the wavelength resolved emission from optically excited NO_2.[5,12,16,18] This would naturally lead to a reduction in observed quantum yield with respect to fluorescence decay rate.

The fate of a single optically excited molecule suffering a collision with a selected set of collision partners is illustrated in Fig. 6. In all cases the most probable event (largest rate constant process) is direct quenching, i.e., collisional conversion of the initial state into nonemitting or undetectable levels. This rate even dominates the pure disalignment rate, important to the interpretation of level crossing[29,30] and double resonance[31] linewidths. This study estimates the pure disalignment rate constant (k_2) for the first time. Collisional production of states with detectable emission (probably vibrationally relaxed $\tilde{A}\,^2B_2$ levels[18]) makes up about 15% of all inelastic processes starting from the optically prepared level. The remaining 85% of the optically excited levels that undergo an inelastic collision exhibit no apparent emission, as recorded by our detector. These NO_2 "dark" levels are thought by us to be high-lying vibrational levels of the ground state, perhaps within kT of the initially prepared level, whose red-shifted fluorescence and lengthened radiative lifetime are caused by mixing to various extents between the NO_2 $\tilde{A}\,^2B_2$ and the $\tilde{X}\,^2A_1$ states. Subsequent collisions continue to modify the set of emitting and dark levels, but these processes are poorly characterized by the experimental methods used in this study.

ACKNOWLEDGMENTS

We thank V. M. Donnelly and F. Kaufman for numerous lively and heated discussions which were truly helpful to us. This work is supported by the National Science Foundation under Grant NSF CHE 81-08823. R.N.Z. gratefully acknowledges support through the Shell Distinguished Chairs Program, funded by Shell Companies Foundation, Inc.

[1] See the references contained in D. K. Hsu, D. L. Monts, and R. N. Zare, *The Spectral Atlas of Nitrogen Dioxide* (Academic, New York, 1978).
[2] D. Neuberger and A. B. F. Duncan, J. Chem. Phys. **22**, 1693 (1954).
[3] L. F. Keyser, F. Kaufman, and E. C. Zipf, Chem. Phys. Lett. **2**, 523 (1968).
[4] Y. Haas, P. L. Houston, J. H. Clark, C. B. Moore, H. Rosen, and P. Robish, J. Chem. Phys. **63**, 4195 (1975).
[5] S. E. Schwartz and H. S. Johnston, J. Chem. Phys. **51**, 1286 (1969).
[6] P. B. Sackett and J. T. Yardley, Chem. Phys. Lett. **6**, 323 (1970).
[7] P. B. Sackett and J. T. Yardley, J. Chem. Phys. **57**, 152 (1972).
[8] V. M. Donnelly and F. Kaufman, J. Chem. Phys. **66**, 4100 (1977).
[9] V. M. Donnelly and F. Kaufman, J. Chem. Phys. **69**, 1456 (1978).
[10] C. H. Chen, S. D. Kramer, D. W. Clark, and M. G. Payne, Chem. Phys. Lett. **65**, 419 (1979).
[11] A. E. Douglas, J. Chem. Phys. **45**, 1007 (1966).
[12] G. H. Myers, D. M. Silver, and F. Kaufman, J. Chem. Phys. **44**, 718 (1966).
[13] K. Sakurai and H. P. Broida, J. Chem. Phys. **50**, 2404 (1969).
[14] L. F. Keyser, S. Z. Levine, and F. Kaufman, J. Chem. Phys. **54**, 355 (1971).
[15] S. Butler, C. Kahler, and D. H. Levy, J. Chem. Phys. **62**, 815 (1975).
[16] V. M. Donnelly and F. Kaufman, J. Chem. Phys. **67**, 4768 (1977).
[17] D. H. Levy, J. Chem. Phys. **68**, 5669 (1978).
[18] V. M. Donnelly, D. G. Keil, and F. Kaufman, J. Chem. Phys. **71**, 659 (1979).
[19] D. G. Keil, V. M. Donnelly, and F. Kaufman, J. Chem. Phys. **73**, 1514 (1980).
[20] P. J. Brucat and R. N. Zare, J. Chem. Phys. **78**, 100 (1983).
[21] R. E. Smalley, L. Wharton, and D. H. Levy, J. Chem. Phys. **63**, 4977 (1975).
[22] The relative velocity of the collision pair in the laboratory frame is not quite isotropic because the line-center narrow-bandwidth laser light selects excited species whose translational motion is near zero along the laser propagation direction (sub-Doppler excitation). The perpendicular components of the velocity of the NO_2 as well all the components of the velocity of the collision partners are not selected. Experiments performed with excitation frequencies not at line center show that this effect is not significant to within our experimental error and the relative velocity of the collision event may be treated as isotropic.
[23] $\langle T^{\dagger}_{20} \rangle$ represents the $k = 2$, $q = 0$ state multipole of the excited state distribution. It is that part of the quadrupole alignment of the molecule's total angular momentum vector that is cylindrically symmetric about the applied field axis.
[24] O. Stern and M. Volmer, Phys. Z. **20**, 183 (1919).
[25] J. Husain, J. R. Wiesenfeld, and R. N. Zare, J. Chem. Phys. **72**, 2479 (1980), T. Carrington, *Eighth Symposium (International) on Combustion* (Williams & Wilkins, Baltimore, 1962).
[26] C. G. Stevens, M. W. Swagel, R. Wallace, and R. N. Zare, Chem. Phys. Lett. **18**, 465 (1973).
[27] J. C. D. Brand and A. R. Hoy, J. Mol. Spectrosc. **65**, 75 (1977).
[28] V. M. Donnelly and F. Kaufman, J. Chem. Phys. **68**, 5671 (1978).
[29] H. Figger, D. L. Monts, and R. N. Zare, J. Mol. Spectrosc. **68**, 388 (1977).
[30] F. Bylicki and H. G. Weber, Chem. Phys. Lett. **79**, 355 (1981).
[31] R. Solarz and D. H. Levy, J. Chem. Phys. **60**, 842 (1974).